Environmental Pollution 323 (2023) 121311

Contents lists available at ScienceDirect

Environmental Pollution

journal homepage: www.elsevier.com/locate/envpol

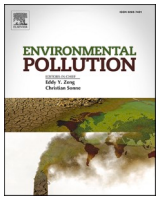

Projections of fire emissions and the consequent impacts on air quality under 1.5 °C and 2 °C global warming☆

Chenguang Tian [a], Xu Yue [a,*], Jun Zhu [a], Hong Liao [a], Yang Yang [a], Lei Chen [a], Xinyi Zhou [a], Yadong Lei [b], Hao Zhou [c], Yang Cao [c]

[a] Jiangsu Key Laboratory of Atmospheric Environment Monitoring and Pollution Control, Collaborative Innovation Center of Atmospheric Environment and Equipment Technology, School of Environmental Science and Engineering, Nanjing University of Information Science & Technology (NUIST), Nanjing, 210044, China
[b] State Key Laboratory of Severe Weather & Key Laboratory of Atmospheric Chemistry of CMA, Chinese Academy of Meteorological Sciences, Beijing, 100081, China
[c] Climate Change Research Center, Institute of Atmospheric Physics, Chinese Academy of Sciences, Beijing, 100029, China

ARTICLE INFO

Keywords:
Fire emissions
$PM_{2.5}$
Ozone
1.5 °C warming
ModelE2-YIBs model

ABSTRACT

Fire is a major source of atmospheric aerosols and trace gases. Projection of future fire activities is challenging due to the joint impacts of climate, vegetation, and human activities. Here, we project global changes of fire-induced particulate matter smaller than 2.5 μm ($PM_{2.5}$) and ozone (O_3) under 1.5 °C/2 °C warming using a climate-chemistry-vegetation coupled model in combination with site-level and satellite-based observations. Compared to the present day, fire emissions of varied air pollutants increase by 10.0%–15.4% at the 1.5 °C warming period and 15.1%–22.5% at the 2 °C warming period, with the most significant enhancements in Amazon, southern Africa, and boreal Eurasia. The warmer climate promotes fuel dryness and the higher leaf area index increases fuel availability, leading to escalated fire flammability globally. However, moderate declines in fire emissions are predicted over the Sahel region, because the higher population density increases fire suppressions and consequently inhibits fire activities over central Africa. Following the changes in fire emissions, the population-weighted exposure to fire $PM_{2.5}$ increases by 5.1% under 1.5 °C warming and 13.0% under 2 °C warming. Meanwhile, the exposure to fire O_3 enhances by 10.2% and 16.0% in response to global warming of 1.5 °C and 2 °C, respectively. As a result, limiting global temperature increase to 1.5 °C can greatly reduce the risks of exposure to fire-induced air pollution compared to 2 °C.

1. Introduction

Fire is an important disturbance inextricably coupled with the climate system, biogeochemical cycles, terrestrial vegetation, and human activities (Chen et al., 2017; Yin et al., 2020). Fire emissions of aerosol particles and trace gases (including greenhouse gases) can modulate atmospheric components (Guo et al., 2017; Hantson et al., 2016; Smolyakov et al., 2014). Fire-emitted aerosols further affect temperature, cloud, and precipitation through both direct and indirect radiative effects (Jiang et al., 2020; Ward et al., 2012; Zou et al., 2020). In addition, fire air pollution influences the ecosystem productivity of unburned forests through ozone (O_3) vegetation damage and aerosol diffuse fertilization (Lei et al., 2021; Yue and Unger, 2018). Changes in land cover by fires influence surface processes by modifying local albedo, evapotranspiration, and soil water capacity (Li et al., 2017; Myhre et al., 2005). Moreover, fires affect human society directly by causing casualties and property losses and indirectly by affecting the air quality of downwind regions (Marlier et al., 2013). The premature death from fire smoke exposure is estimated to be 339,000 each year on the global scale (Johnston et al., 2012).

Climate is a dominant driver of fire activities through modulating fire weather, plant growth, and fuel moisture (Andela et al., 2017). Humans have also shaped the global burning pattern for millennia (Bowman et al., 2009). Currently, human activities are the leading ignition source in tropical fire-prone regions (Aragão et al., 2008; Archibald et al., 2009). Changes in climate and human activities have shown large impacts on fire activity. For example, significant increases in both fire number and burned area (BA) were found in the U.S. during 1984–2011 mainly because of climate changes (Dennison et al., 2014). Globally, fire season length was extended by 18.7% from 1979 to 2013 following the

☆ This paper has been recommended for acceptance by Pavlos Kassomenos

* Corresponding author.
E-mail address: yuexu@nuist.edu.cn (X. Yue).

https://doi.org/10.1016/j.envpol.2023.121311
Received 14 November 2022; Received in revised form 10 February 2023; Accepted 16 February 2023
Available online 17 February 2023

changes in temperature and humidity (Jolly et al., 2015), while BA declined by 25% from 1998 to 2015 due to human activities (Andela et al., 2017).

Given the important roles of fire, many efforts have been made to project future changes in fire activities under global warming in the 21st century (Table 1). While different studies project different impacts of climate on fire emissions, there is a general consensus that there will be more fire activity and a longer fire season length. Most previous studies relied on empirical/statistical models or fire weather indexes that ignore the joint impacts of climate and human activities. Furthermore, no studies have investigated the changes in future fire emissions and the resulting effects on air quality under specific warming targets such as 1.5 °C and 2 °C, which were set by the 2015 Paris Agreement to mitigate global warming. Many previous studies have shown that the additional half-degree warming would result in severe dangers, including more weather and climate extremes (King et al., 2017), declined Arctic sea ice (Jahn, 2018), accelerated permafrost loss (Chadburn et al., 2017), and rising sea level (Schleussner et al., 2016).

Considering the significance of these temperature thresholds, we project future changes in fire emissions and the consequent impacts on aerosols and surface O_3 under the 1.5 °C and 2 °C warming levels by using a well-developed active fire parameterization implemented in the coupled climate-chemistry-vegetation model ModelE2-YIBs (Tian et al., 2022; Yue and Unger, 2015). Both site-level observations and satellite retrievals are collected to evaluate the model. The simulated future climate is compared with the multi-model ensemble (MME) projections from phase 6 of Coupled Model Intercomparison Project (CMIP6). With these configurations, we expect to derive robust projections of future fire emissions to better understand the influences of fires on ecosystems, air quality, and public health in a low-warming world.

2. Data and methods

2.1. Datasets

2.1.1. Fire emissions

The Global Fire emission database version 4.1s (GFED4.1s) averaged for 2000–2010 is employed to validate the performance of the fire parameterization at the present day. GFED4.1s inventory provides global estimates of monthly BA and fire emission fluxes derived from satellite retrievals from Moderate Resolution Imaging Spectroradiometer (MODIS) (van der Werf et al., 2017). For the MODIS era, total BA is the combination of the MCD64A1 BA product (Giglio et al., 2013) based on MODIS surface reflectance and the small-fire BA layer (Randerson et al., 2012) based on active-fire detections. For the pre-MODIS era, statistical relationships of the active-fire detections between MODIS and Visible and Infrared Scanner (VIRS) (Giglio et al., 2003) and the European Space Agency Advanced Along Track Scanning Radiometer (ATSR) (Arino et al., 1999) are developed to estimate BA. The gridded fire emission dataset is available from July 1997 onwards, with a spatial resolution of 0.25° × 0.25°.

2.1.2. Aerosol optical depth (AOD)

We use monthly observations of AOD at 550 nm from MODIS retrievals during 2000–2010 for model validations at the present day. The MODIS instruments onboard Aqua and Terra view the whole Earth's surface every 1–2 days with a 2330 km swath at 36 spectral bands. The well-known Dark Target algorithm is employed to estimate AOD over dense and dark terrestrial vegetation (Kaufman et al., 1997; Levy et al., 2013). Meanwhile, the Deep Blue algorithm is used to estimate AOD over the bright land surface (Hsu et al., 2004). Over the ocean, another "Dark Target" approach is applied (Tanré et al., 1997). The spatial resolution of the MODIS collection 6.0 AOD dataset is 10 × 10 km.

2.1.3. Site-level O_3 measurements

Three observational networks are utilized to evaluate simulated O_3

Table 1
Summary of studies projecting future wildfire activities.

Metric	Area	Method	Results	Reference
Fire weather	North America	Index	Fire seasonal severity rating increases by 10–50% in the 2050s	Flannigan et al. (2000)
BA[a]	Western Canada	BORFIRE model	Increases by 14–137% in 2080–2100 compared with 1975–1990	Groot et al. (2003)
Occurrence	Canada	Index	Increases by 34% by 2061–2100 compared to the past two centuries	Girardin and Mudelsee (2008)
Occurrence	Global	Statistical model	Changes by 0.5–2.8 in the A2 scenario and 0.7–1.9 in B1 scenario[b]	Krawchuk et al. (2009)
Fire weather	Portugal	Index	Available burnable area increases from 1.4% to 7.8% under the 2 × CO_2 scenario	Carvalho et al. (2009)
Fire regime	Australia	Statistical model	Although increases occur in temperate forests, rising dryness may diminish fire activity	Bradstock (2010)
Fire potential	Global	Index	Fire potential will increase from moderate to high in southern Africa, South America, and Australia, with a longer high fire potential period from 2 to 8 months	Liu et al. (2010)
Fire activity	Mediterranean ecosystems	Statistical model	Substantial decreases under a warmer and drier future	Batllori et al. (2013)
Fire season	Global	Statistical model	Annual fire season lengths in northern high latitudes increase by > 20 days	Flannigan et al. (2013)
BA	Southern California	Statistical model	Doubles in Southwestern California by 2050, increases by 35% in the Sierra Nevada and 10% in central western California compared with 1981–2000	Yue et al. (2014)
Fire emission	Europe	LPJ-GUESS model	A moderate increase in fire emissions is plausible until 2050. A doubling of fire emissions in the late 21st century is possible under higher CO_2	Knorr et al. (2016)

(continued on next page)

Table 1 (*continued*)

Metric	Area	Method	Results	Reference
			emissions trajectories	
BA	Western US	Statistical model	Increases by 88%–116% in 2071–2100 compared with 1981–2010	Liu and Wimberly (2016)
Fire-induced air pollution	Global	LPJ-GUESS and CAM-CHEM model	During the high-fire season, future PM2.5 pollution levels can reach hazard levels even for the scenario with an aggressive reduction of anthropogenic emissions.	Knorr et al. (2017)
Fire-induced air pollution	North America	ModelE2-YIBs model	Summer O_3 enhances 2 ppbv and AOD enhances 0.03 in 2050s compared to 2010s	Yue et al. (2017)
BA	Mediterranean Europe	Empirical formula	Increases by 40–54% for 1.5 °C of global warming, 62–87% for 2 °C and 96–187% for 3 °C	Turco et al. (2018)
Fire weather	Global	index	Increases 11–40% by 2050s compared to 2019 and double at 3 °C compared with 2 °C	Abatzoglou et al. (2019)
Probability	Brazilian Amazon	Statistical model	RCP 4.5 + Sustainability: increase by 21.3%; RCP 8.5 + Sustainability: increase by 39.1%; RCP 8.5 + Fragmentation: increase by 113.5% in October by 2071–2100	Fonseca et al. (2019)
BA	Brazilian *Cerrado*	Statistical model	Increases by 0.9 $\times 10^6$ ha in 2071–2100 under RCP2.6, 3.16 under RCP4.5, and 7.71 under RCP8.5 scenario compared to 1976–2005	Silva et al. (2019)
Fire-induced air pollution	Western U.S.	LPJ-LMfire model	BC/OC increase by 0.18 Tg month^{-1} under RCP4.5 scenario and 0.39 Tg month^{-1} under RCP8.5 scenario in 2100s compared to 2010s	Li et al. (2020)
Fire weather	Global	Index	Half-degree warming may lead to significant increases in wildfires in parts of the world, such as the Amazon, African savanna, and the Mediterranean	Son et al. (2021)
BA	Global	IMOGEN-LPJ-SEVER model	Decreases 0.03 Mha year^{-2} in S1 scenario but increases by 1.69 Mha year^{-2} in S2, 0.58 Mha year^{-2} in S3, and 0.88 Mha year^{-2} in S4 scenarios[c]	Wu et al. (2021)
Fire-induced air pollution	Western U.S.	WRF-CMAQ model	small changes in regional averaged air pollutant concentrations, while large increase in city-scale air pollutant concentrations	Yang et al. (2022)

[a] BA: burned area.
[b] A2 and B1 are scenarios used in CMIP3.
[c] S1–S4 scenarios are combinations of CO_2 emissions using RCP (2.5, 4.5 or 8.5) and population using SSP (2, 3 or 5).

concentrations at the present day, including the Clean Air Status and Trends Network (CASTNET) in the U.S., the European Monitoring and Evaluation Programme (EMEP) in Europe, and the Air Quality Monitoring Network from the Ministry of Ecology and Environment (AQMN-MEE) in China. All datasets are averaged over 2010 except for AQMN-MEE, which is averaged over 2014. This is because the AQMN-MEE network, which started in 2013, produced high-quality data since 2014. Modeled O_3 are bilinearly interpolated to the locations of observational sites.

2.1.4. CMIP6 dataset

Climate datasets from 19 CMIP6 models (Eyring et al., 2016) are selected as boundary forcing and model validations (Table S1). We select surface air temperature (SAT), precipitation, sea surface temperature (SST), and sea ice fraction (SIC) from both historical periods (1850–2014) and the shared socioeconomic pathways (SSP) 5–8.5 scenario (2015–2100), a combination of SSP5 with fossil-fueled development and Representative Concentration Pathways (RCP) 8.5 with high radiative forcing. In the SSP5-8.5 scenario, anthropogenic radiative forcing will reach 8.5 W m^{-2} by 2100, depicting a high end of global warming (Eyring et al., 2016). For each model, only the member 'r1i1p1f1' is considered.

2.1.5. Population density

Global downscaled population datasets (Gao, 2017, 2020) are employed to derive both anthropogenic ignitions and suppressions. The dataset provides global urban, rural, and total population density in 2000, and projects future population from 2010 to 2100 at decadal intervals and a spatial resolution of 1 × 1 km. We select the future projection developed for the SSP5-8.5 scenario.

2.2. ModelE2-YIBs model

The NASA Goddard Institute for Space Studies (GISS) ModelE2 is a state-of-the-art climate model with a spatial resolution of 2° × 2.5° and 40 vertical layers extending to 0.1 hPa. The model calculates the dynamic and physical processes every 0.5 h and the radiation module is called every 2.5 h. It simulates tropospheric chemistry including the canonical NO_x-HO_x-O_x-CO-CH_4 chemistry and a large number of volatile organic compound (VOC) species. The radiation package of the model is used to interactively calculate the effects of aerosols such as nitrate, sulfate, sea salt, dust, black carbon (BC), and organic carbon (OC),

which affect the climate system through both direct and indirect effects. The model has been widely validated for both meteorological and hydrological variables with observations and reanalysis datasets and is extensively employed to investigate the atmospheric components, climate change, and their interactions (Schmidt et al., 2014). More detailed information about ModelE2 can be obtained from Schmidt et al. (2014).

The Yale Interactive terrestrial Biosphere model (YIBs) is a process-based vegetation model developed by Yue and Unger (2015). YIBs dynamically simulate changes in the leaf area index (LAI) and the land carbon cycle. There are nine plant functional types (PFTs) embedded in YIBs, including evergreen broadleaf forest, deciduous broadleaf forest, evergreen needleleaf forest, shrubland, C_3/C_4 grass, C_3/C_4 cropland, and tundra. Essential ecological processes such as leaf-level photosynthesis, canopy radiative transfer, phenology, and plant and soil respiration are incorporated and parameterized in YIBs. The previous study showed that simulated gross primary productivity (GPP) agreed well with site measurements and simulated tree height, LAI, phenology, and carbon fluxes were consistent with satellite retrievals (Yue and Unger, 2015). Recently, YIBs joined the vegetation model intercomparison project TRENDY and demonstrated good performance in simulating key parameters in the carbon cycle (Friedlingstein et al., 2020).

Yue and Unger (2015) implemented YIBs to ModelE2 and built a two-way coupled climate-chemistry-vegetation model (ModelE2-YIBs). ModelE2 provides meteorological drivers to YIBs, and YIBs affects the atmosphere by altering the land surface energy balance through ecosystem processes. The new climate-vegetation model, based on coupled YIBs and ModelE2 models, can simulate terrestrial ecosystem feedback to climate systems via energy, water, and chemistry exchanges (Yue et al., 2017; Yue and Unger, 2015).

2.3. Fire parameterization

The active global fire parameterization developed by Pechony and Shindell (2009) was implemented into the ModelE2-YIBs in our previous study (Tian et al., 2022). The parameterization is composed of several important fire-related factors such as fuel flammability, ignition sources, and anthropogenic suppressions. A brief introduction to the parameterization is provided as follows.

The formulation of trace gases and particulate matters emitted by fire ($Emission_{fire}$) is represented as:

$$Emission_{fire} = N_{fire} \times EF \quad (1)$$

Here, the emissions of BC, OC, carbon monoxide (CO), nitrogen oxides (NO_x), methane (CH_4), Alkenes, and Paraffin are represented by EF. N_{fire} (unit: number km^{-2}) is the fire count density:

$$N_{fire} = FF \times (I_N + I_A) \times f_{NS} \quad (2)$$

FF is fuel flammability standing for the conditions favorable for fire occurrence, tightly coupled with precipitation (Pr, unit: day mm^{-1}), vapor pressure deficit (VPD, unit: hPa), and LAI (unit: $m^2\ m^{-2}$):

$$FF = e^{-2\times Pr} \times VPD \times LAI \quad (3)$$

Natural ignition I_N is determined by cloud-to-ground lightning, which is estimated by the ModelE2 model. Anthropogenic ignition I_A is expressed as:

$$I_A = 0.03 \times k(PD) \times PD \quad (4)$$

where PD is population density (unit: number km^{-2}) and the anthropogenic ignition potential is represented by $k(PD) = 6.8 \times PD^{-0.6}$. The fraction of non-suppressed fires f_{NS} is calculated as:

$$f_{NS} = 0.05 + 0.9 \times \exp(-0.05 \times PD) \quad (5)$$

2.4. Simulations

We use ModelE2-YIBs to project future fire emissions in a warmer climate with prescribed boundary conditions following the same strategy as Atmospheric Model Intercomparison Project (AMIP) (Gates et al., 1999). Dynamic fire parameterization has been implemented into ModelE2-YIBs, as shown in Section 2.3. Population density from the global downscaled population dataset, and MME mean CO_2 concentrations ($[CO_2]$ hereafter) and SST/SIC from CMIP6 models at the present or 1.5/2 °C warming periods are derived as model boundary conditions. The details are as follows.

We use the decadal average of 1995–2005 (HIST) to represent the present-day state. The periods reaching 1.5 °C and 2 °C warming for each model from CMIP6 (Fig. S1 and Table S1) are then calculated using the combination of historical and SSP5-8.5 scenarios. SAT is smoothed over an 11-year running-mean window for each model and the different warming periods are defined as the time when the global average SAT is 1.5 °C or 2 °C higher than the preindustrial level (PI, 1850–1900). The warming periods show great variations among CMIP6 models with the earliest appearance of 1.5 °C warming in the 1990s for CIESM and the latest in the 2040s for NorESM2-LM (Table S1). We then derive the population density (Fig. S2) from the global downscaled population dataset, and MME $[CO_2]$ and SST/SIC (Fig. S3) from 19 CMIP6 models for warming periods of 1.5 or 2 °C.

We conduct eight time-slice simulations to quantify the effects of 1.5 or 2 °C global warming on fire emissions and the consequent perturbations in air pollution (Table 2). In these simulations, fire-induced O_3 and aerosol loadings are dynamically simulated with atmospheric chemistry processes, which are fully coupled with atmospheric circulation and the terrestrial ecosystem. Experiments are split into three groups: (1) In the first group, three baseline experiments without fire emissions ('NF') are forced using boundary conditions from the HIST, 1.5 °C, and 2 °C periods, respectively. (2) The second group is the same as the first group except that all simulations include fire emissions ('YF'). (3) In the third group, two runs including fire emissions are driven by climatic boundary conditions (CO_2 and SST/SIC) at the 1.5 °C and 2 °C periods, but with population density fixed at HIST period. For example, simulation "HIST_YF" turns on fire emissions for the historical period while "1PT5_NF" run turns off fire emissions in the 1.5 °C warmer world. By comparing HIST_YF with HIST_NF, we can derive the contributions of fire emissions to atmospheric components in the present day. The changes in fire emissions under global warming are calculated from the corresponding future and HIST experiments. By calculating the differences between the second and third groups, the effects of human activities and climate change to fire emissions can be further separated. All simulations are integrated for 25 years, with the last 20-year average for analyses. A two-tailed Student's *t*-test is performed to assess the significance of all differences. The population-weighted exposure to fire $PM_{2.5}$ is defined as:

$$\text{exposure} = \frac{\Sigma(PD \times FirePM_{2.5})}{\Sigma PD} \quad (6)$$

where $FirePM_{2.5}$ is fire-induced surface $PM_{2.5}$ concentrations. Both PD and $FirePM_{2.5}$ are gridded data at the same spatial resolution of 2° ×

Table 2
Summary of simulations using ModelE2-YIBs.

Simulations	SST/SIC	GHGs	Population	Fires
HIST_NF	HIST	HIST	HIST	No
1PT5_NF	1.5 °C	1.5 °C	1.5 °C	No
2PT0_NF	2.0 °C	2.0 °C	2.0 °C	No
HIST_YF	HIST	HIST	HIST	Yes
1PT5_YF	1.5 °C	1.5 °C	1.5 °C	Yes
2PT0_YF	2.0 °C	2.0 °C	2.0 °C	Yes
1PT5_HISTPD_YF	1.5 °C	1.5 °C	HIST	Yes
2PT0_HISTPD_YF	2.0 °C	2.0 °C	HIST	Yes

2.5°.

3. Results

3.1. Model evaluations

The simulated fire-emitted BC and OC in experiment "HIST_YF" are compared with observations from GFED (Fig. 1). With distinct dry season and/or abundant vegetation, the highest fire emissions are both observed and simulated in the tropical regions. Although ModelE2-YIBs slightly overestimates fire emissions in the Amazon while it underestimates emissions in central Africa, the model adequately captures the spatial distribution when compared to GFED with low model-to-observation differences. Globally, ModelE2-YIBs simulates annual fire emissions of 1.92 Tg (1 Tg = 10^{12} g) C for BC and 17.1 Tg C for OC, comparable to the satellite-based observations of 1.86 Tg C and 16.4 Tg C respectively. The normalized mean bias (NMB) is 3.4% for BC and 4.3% for OC with spatial correlation coefficients of 0.71 ($p < 0.01$) and 0.61 ($p < 0.01$), respectively.

We then evaluate AOD at 550 nm and surface O_3 in ModelE2-YIBs (Figs. S4–S5). The model successfully reproduces the observed geographic distribution of AOD, including high values in Africa, South Asia, and East Asia. Globally, a high correlation of 0.91 ($p < 0.01$) and a low NMB of 2.82% are derived between simulations and observations

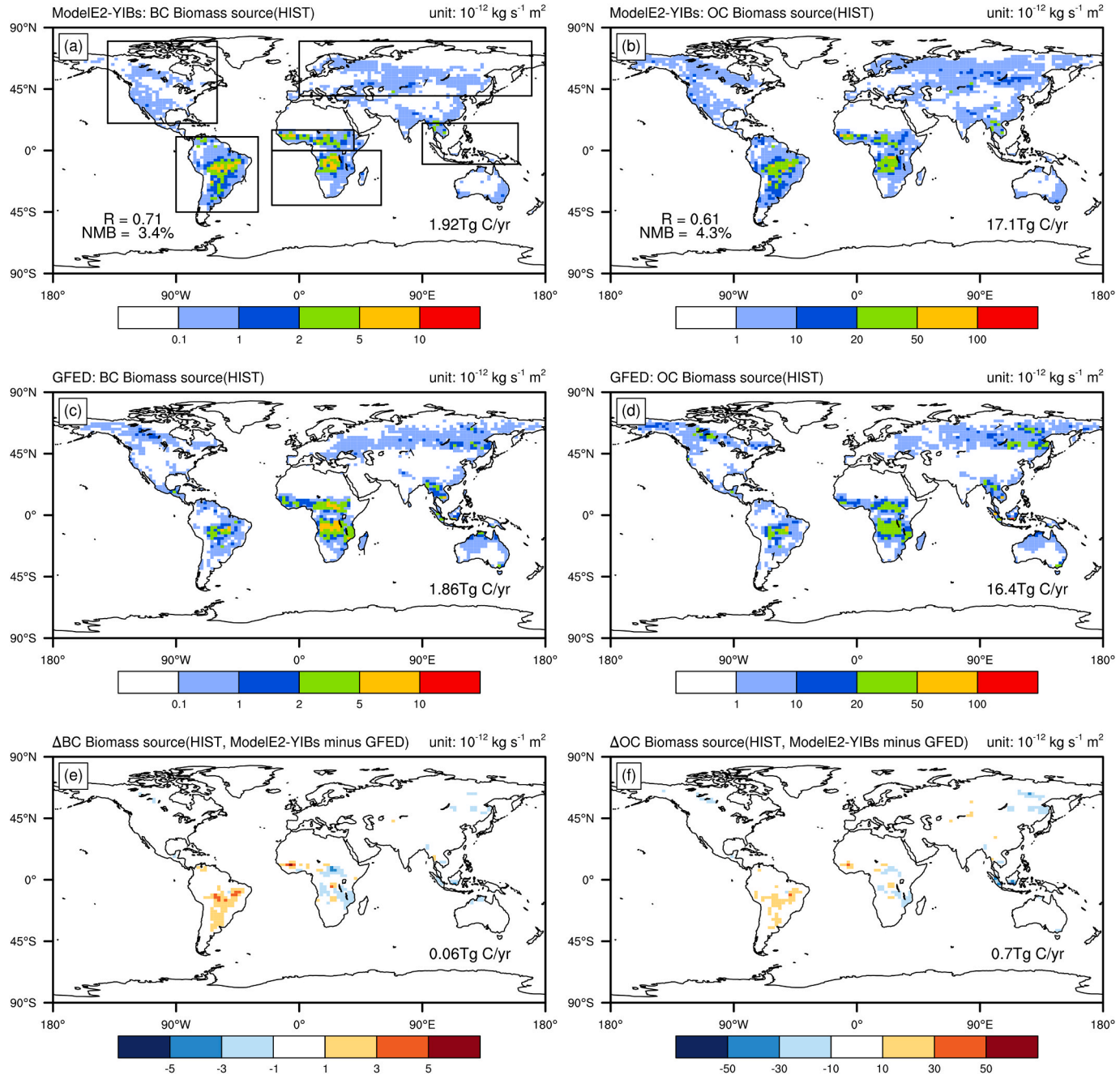

Fig. 1. Annual mean fire emissions of (left) BC and (right) OC from (a, b) ModelE2-YIBs, (c, d) GFED4s, and (e, f) their differences (model minus observations) at the present day (HIST). Modeling results are from the control simulation of HIST_YF. The total emissions are shown on the bottom right of each panel. The correlation coefficients (R) and normalized mean biases (NMB) between simulations and observations are shown on the top panels. The boxes in (a) represent sub-regions shown in Fig. S8.

(Fig. S4). Regionally, the differences between ModelE2-YIBs and the observations are generally small though the model overestimates AOD in the Sahel while underestimates it in central Africa and East Asia.

Surface daily maximum 8-h average O_3 concentrations (MDA8-O_3, abbreviated as [O_3] hereafter) are evaluated using *in situ* observations from the ground-based network (Fig. S5). ModelE2-YIBs overestimates [O_3] by 10–15 ppbv in western Europe and the eastern U.S., both of which are densely urban areas. Such discrepancy may be attributed to the coarse model resolution that fails to distinguish [O_3] between urban and rural areas. Simulated [O_3] matches observations on a global scale with a correlation coefficient of 0.46 ($p < 0.01$) and NMB of 20.41%. Gong et al. (2020) compared ModelE2-YIBs with six state-of-the-art earth system models participating in the Atmospheric Chemistry and Climate Model Intercomparison Project (ACCMIP) and found that ModelE2-YIBs has comparable performance to other models in the simulation of surface O_3.

3.2. Fire-induced perturbations in aerosols and O_3 at the present day

Fire emissions primarily increase surface aerosols and O_3 in tropical regions (Fig. 2). Hotspots are located in low-latitude regions, especially South America and southern Africa. In addition, large enhancement is found in boreal high latitudes. For AOD, the regional rise is larger than 0.05 in central Africa and Amazon. Globally, fires increase AOD by 0.007 on the annual mean basis with the terrestrial enhancement of 0.011. At the surface, fires enhance the concentrations of particulate matter smaller than 2.5 μm ($PM_{2.5}$) by 0.29 μg m^{-3} globally with 0.63 μg m^{-3} over land area, resulting in population-weighted exposure of 0.52 μg m^{-3} to fire $PM_{2.5}$. The largest enhancement of >5 μg m^{-3} is located in the southern Amazon. For surface O_3 which is formed indirectly through the photochemical reactions among fire-emitted precursors, the presence of fires elevates the surface [O_3] by 2.52 ppbv globally and 3.79 ppbv over land, with 2.26 ppbv for population-weighted exposure. A large [O_3] enhancement of >15 ppbv is located in South America and southern Africa, consistent with the predictions by Yue and Unger (2018) using a different chemical transport model.

3.3. Projection of future climate change

Simulated changes in annual terrestrial SAT and precipitation are compared with the CMIP6 models (Fig. S6). Under 1.5 °C warming, ModelE2-YIBs simulates widespread enhancement in SAT with a relatively larger magnitude in high latitudes (Fig. S6a). A similar pattern is exhibited during the 2 °C warming period with a much stronger magnitude (Fig. S6b). On the global mean basis, land SAT increases by 0.89 °C (1.46 °C) at 1.5 °C (2 °C) warming level compared to the present day. Such findings are analogous to the MME from CMIP6 models (Figs. S6c–d) with spatial correlations of 0.93 (0.96) and NMB of −3.8% (−8.7%) over land areas under 1.5 °C (2 °C) warming.

Projected changes in precipitation over land areas by the ModelE2-YIBs model generally resemble those by CMIP6 MME under global warming (Fig. S7). Enhancements of precipitation are predicted over North America, Eurasia, and central Africa while decreases are found in the Southern Hemisphere under 1.5 °C warming (Fig. S7a). Precipitation changes in the 2 °C warmer climate show similar spatial patterns as those under 1.5 °C warming conditions (Fig. S7b). Compared to the present day, global average land precipitation increases by 0.39 mm/month and 0.90 mm/month in the 1.5 °C and 2 °C warmer world, respectively. These changes are consistent with the MME from CMIP6 models (Figs. S7c–d) with spatial correlations of 0.40 and 0.45. The ModelE2-YIBs in general predict larger regional perturbations in precipitation than CMIP6 MME, likely because the latter has smoothed the

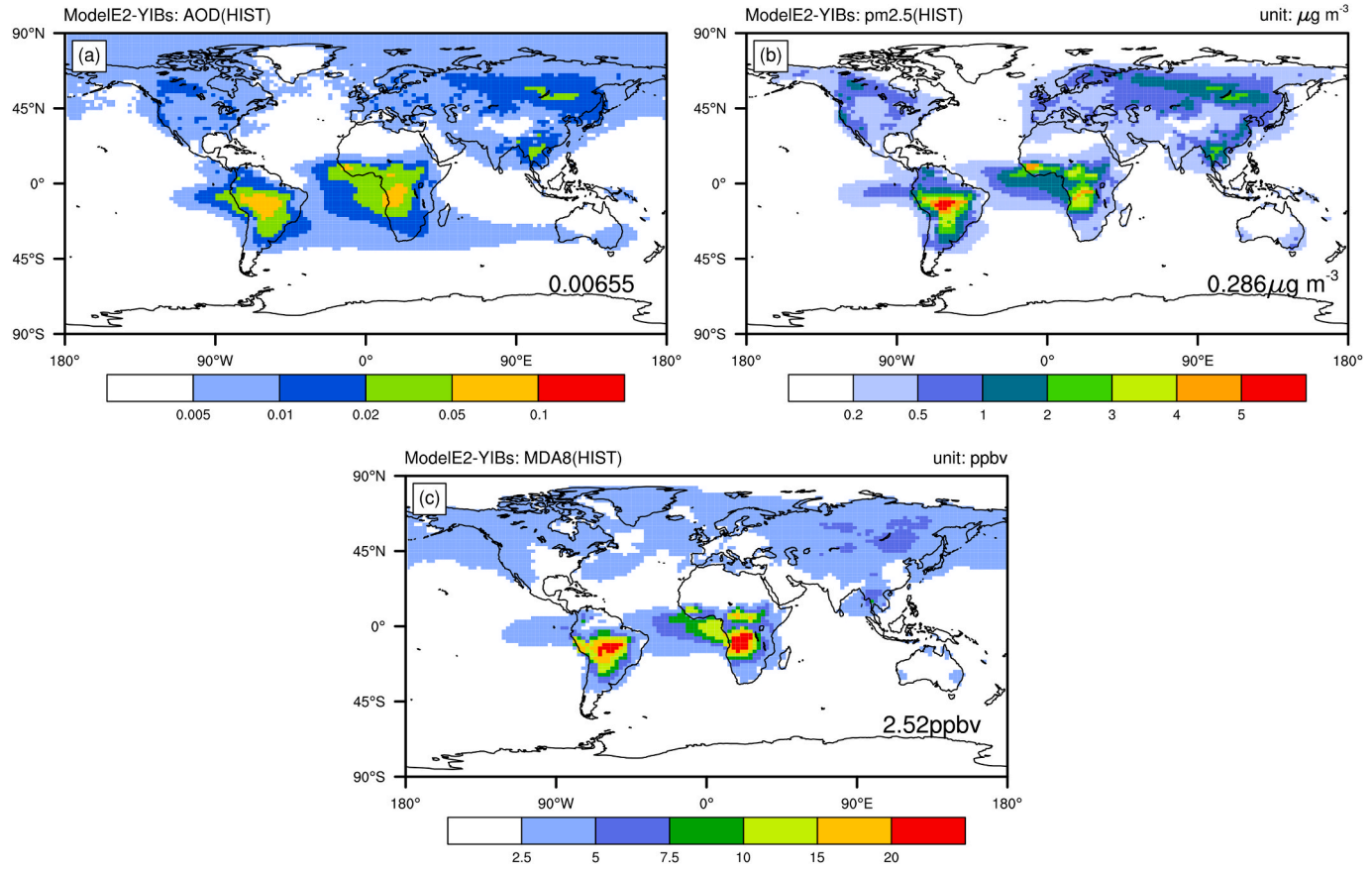

Fig. 2. Annual mean (a) AOD at 550 nm, (b) surface $PM_{2.5}$, and (c) surface MDA8 O_3 concentration induced by fire at the present day.

variability among different models (Figs. S7c–d).

3.4. Projection of future fire emissions and air pollution

In response to the global warming of 1.5 °C, fire emissions show widespread enhancements of 0.5–1.5 × 10^{-12} kg s^{-1} m^{-2} for BC and 5–15 × 10^{-12} kg s^{-1} m^{-2} for OC over tropical rainforests and Africa savannas, respectively (Fig. 3a and b). By 2 °C warming, ΔBC and ΔOC exhibit similar distribution as those in 1.5 °C but with a larger magnitude (Fig. 3c and d). Regionally, fire-emitted BC is predicted to increase by 16.7% (23.2%) in South America, 22.6% (24.8%) in North America, 12.5% (30.5%) in boreal Eurasia, 3.2% (4.6%) in Africa and 6.4% (11.9%) in Southeast Asia under 1.5 °C (2 °C) warming (Fig. S8). A similar magnitude of changes is projected for fire-emitted OC. The small increases in Africa result from the opposite changes in the Sahel and South Africa, where fire-emitted BC increases by 7.42% (12.8%) and decreases by 1.43% (4.4%) at the 1.5 °C (2 °C) warming, respectively. On the global scale, BC emissions from fires increase by 9.98% (15.05%) at the 1.5 °C (2 °C) warming period compared to the present day. Similarly, fire-emitted OC increases by 11.9% (17.6%) in a 1.5 °C (2 °C) warmer world. Other pollutant species emitted by fires also increase by 11.2%–15.6% at 1.5 °C and 16.6%–22.5% under 2 °C warming levels (Table 3).

Changes in fire-related air pollutants mainly follow that of fire emissions under global warming (Fig. 4a-b). The largest increase of fire-induced AOD is found in South America with a regional maximum of 15.5% and 17.5% under 1.5 °C and 2 °C warmings, respectively. However, there is a slight reduction in the Sahel owing to decreased fire emissions (Fig. 3). Globally, fire-induced AOD on average increases by 0.00083 (12.6%) at 1.5 °C warming level and 0.00112 (17.1%) at 2 °C warming level. Fire-induced changes in $PM_{2.5}$ show similar patterns as those in AOD with global average changes of 0.024 μg m^{-3} (8.4%) by 1.5 °C warming and 0.032 μg m^{-3} (11.2%) by 2 °C warming (Fig. 4c-d). The population-weighted exposure to fire $PM_{2.5}$ increases by 0.027 μg m^{-3} (5.1%) at the 1.5 °C warming period and 0.068 μg m^{-3} (13.0%) at the 2 °C warming period. The more than doubled enhancement in fire $PM_{2.5}$ exposure with additional half-degree warming is in part related to the larger population density in a 2 °C warming world compared to 1.5 °C. Fire-induced [O_3] is enhanced at almost all terrestrial grids (Fig. 4e-f). The largest increases are mainly located in South America and southern Africa. At the regional scale, fire [O_3] is predicted to increase by 10.5% in North America, 15.2% in South America, and 4.9% in Africa at the 1.5 °C warming. These changes are 14.3%, 20.1%, and 7.6% at the 2 °C warming. Elevated fire [O_3] promotes population exposure by 10.2% under 1.5 °C warming and 16.0% under 2 °C warming.

3.5. Drivers of future changes in fire activity

Fire activity is subject to a complicated combination of natural and anthropogenic factors. Under global warming, VPD shows widespread enhancements (Fig. 5a and b) due to higher temperature (Figs. S6a–S6b) and changes in precipitation (Figs. S7a–S7b). The increased VPD promotes fuel dryness and contributes to larger flammability (Equation (1)), not to mention that higher temperatures elongate fire seasons (Jolly et al., 2015). Meanwhile, increases in LAI (Fig. 5c–d) due to CO_2 fertilization (Tian et al., 2021) promote fuel availability and further enhance global fire activities. Furthermore, lightning ignitions increase by 6.3% under 1.5 °C and raise by 10.8% at 2 °C warming (Fig. 5e–f), likely because of the enhanced atmospheric convective available

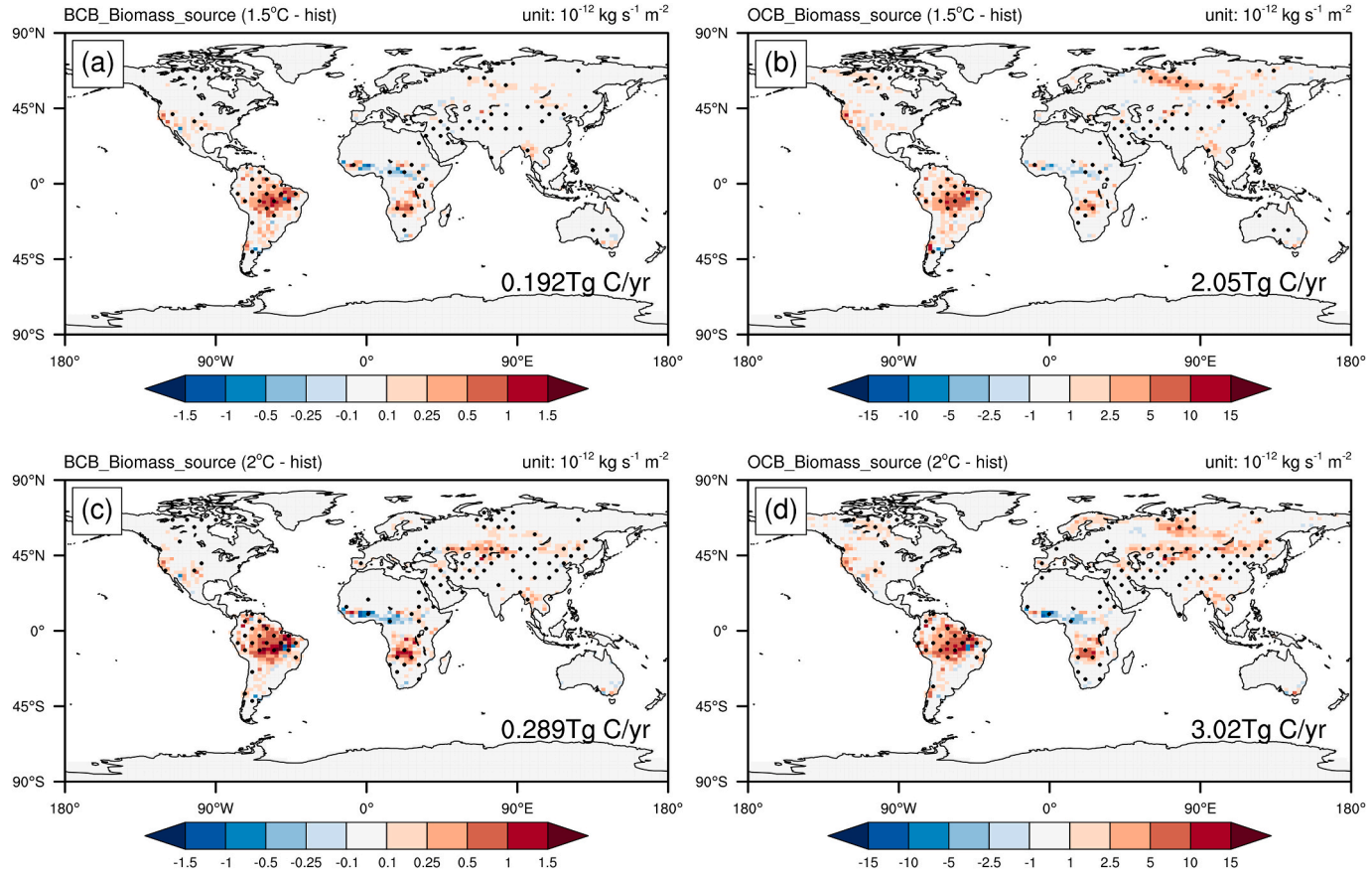

Fig. 3. Annual mean changes in fire-induced (left) BC and (right) OC emissions by (a, b) 1.5 °C and (c, d) 2 °C warming compared to the present day. Dots denote areas with significant ($p < 0.1$) changes.

Table 3
Annual global fire emissions.

	BC	OC	NO_x	CO	CH_4	Alkenes	Paraffin
HIST (Tg)	1.92	17.1	6.66	376.1	14.8	0.334	0.186
1.5 °C (Tg)	2.11	19.2	7.30	420.6	17.1	0.376	0.208
2 °C (Tg)	2.21	20.1	7.65	442.1	18.1	0.397	0.220
1.5 °C - HIST	10.0%	12.0%	11.2%	11.9%	15.4%	12.6%	15.6%
2 °C - HIST	15.0%	17.6%	16.6%	17.6%	22.4%	18.6%	22.5%

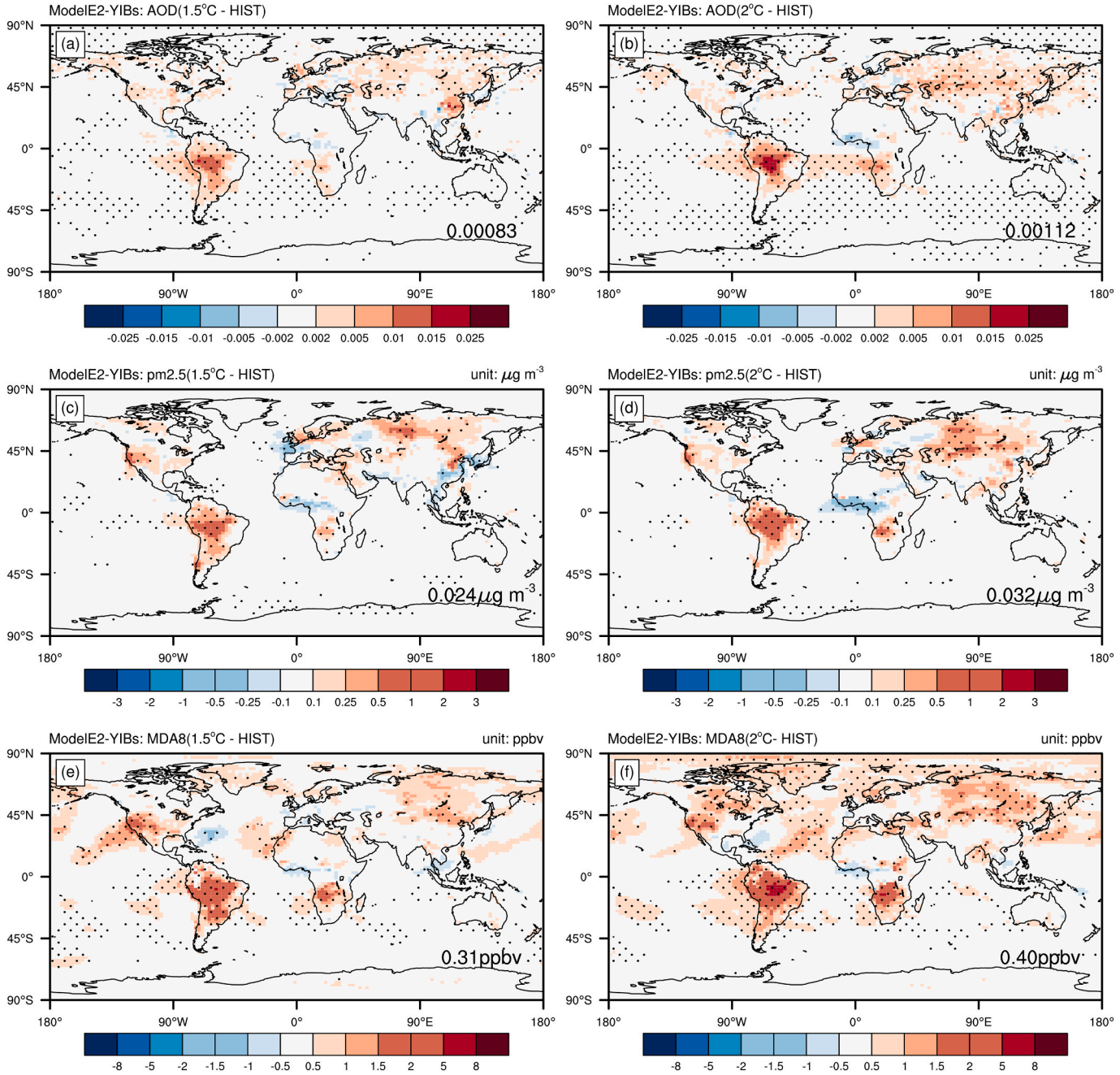

Fig. 4. Annual mean changes of (top) AOD at 550 nm and (middle) surface $PM_{2.5}$ and (bottom) surface MDA8 O_3 concentration induced by fire by (a, c, e) 1.5 °C and (b, d, f) 2 °C warming compared to present day. Dots denote areas with significant ($p < 0.1$) changes.

potential energy (Chen et al., 2020) and increased cloud top height (Clark et al., 2017) or more favorable climatic conditions (Price, 2009) in a warming climate. Consequently, climate change promotes global fire emissions (Fig. S9).

Human activities have both positive and negative effects on the occurrence of fires. Their joint effects show obvious spatial heterogeneity with large reductions in Eurasia and central Africa at both warming targets (Fig. 5g–h). The negative effects of human activities in Eurasia are related to fewer ignitions (Fig. S10) following reduced population density (Fig. S2). However, reduced fire activities in central

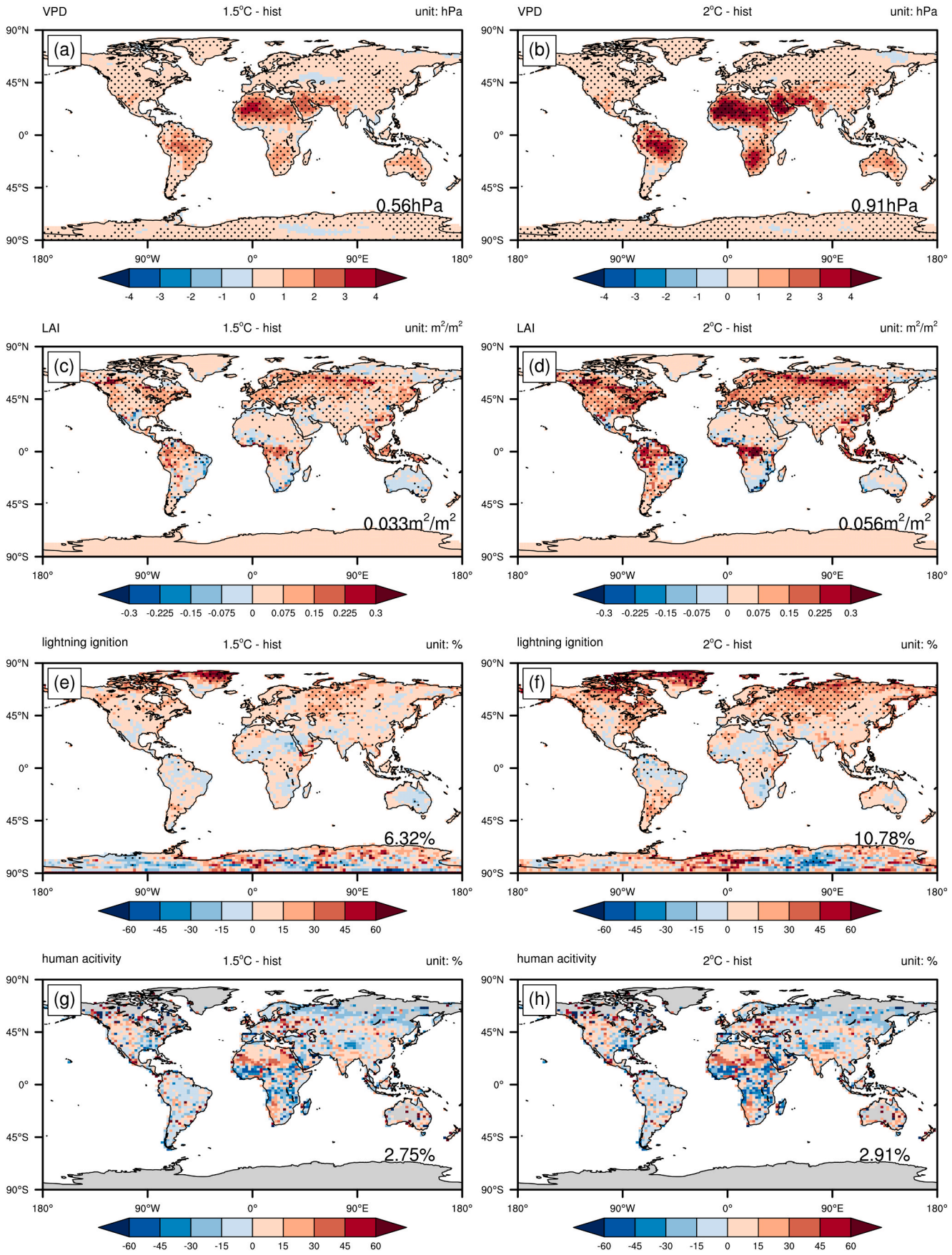

Fig. 5. Annual mean changes in (a, b) VPD, (c, d) LAI, and relative changes (unit: %) in (e, f) lightning ignition and (g, h) the impact of human activities on fires (including both ignition and suppression) over land grids under (left) 1.5 °C and (right) 2 °C warming. Dots denote areas with significant ($p < 0.1$) changes in (a–f).

Africa are mainly attributed to increased fire suppressions (Fig. S10) due to nearly doubled population density (Fig. S2). Such changes are in accordance with the recent trends in global BA from satellite observations (Andela et al., 2017). Consequently, fire-induced $PM_{2.5}$ shows reductions in the Sahel, partly offsetting the increases of fire particles elsewhere (Fig. 4c-d). Globally, the net contribution of future anthropogenic activities slightly inhibits global wildfire emissions (Fig. S11), partially offsetting the promoting effect of climate change (Fig. S9). Therefore, the joint effects of climatic change and human activities result in a global increase in fire emissions with regional reductions under 1.5 °C and 2 °C warmings.

4. Discussion

The projections from this study show increased fire activities under a warmer climate, consistent with many previous assessments at regional and global scales (Table 1). These changes are attributed to the higher temperature, larger VPD (or lower relative humidity), and more fuel availability under global warming. However, fire emissions are not uniformly increased and regional reductions are predicted in central Africa. Such reductions are likely robust as satellite data showed similar decreasing trends in African fires over the past two decades (Andela et al., 2017). Abatzoglou et al. (2019) also found extreme fire activities will be more frequent under global warming except for equatorial Africa. Besides, Knorr et al. (2017) showed that demographic changes were the primary drivers of the fire emission change in sub-Saharan Africa under global warming. Compared to the 1.5 °C warming, our projections show that the increment of fire emissions is larger by 50% and the population-weighted exposure to fire $PM_{2.5}$ is higher by 160% under the 2 °C warming. Son et al. (2021) also found that the additional half-degree warming might lead to a significantly increased regional fire hazard, particularly in the Amazon. Considering the large spatial heterogeneity, we expect more regional pollution episodes caused by fires in a warmer climate. Accordingly, population exposure to fire pollutants increases in the future, with substantial increment in 2 °C warming relative to 1.5 °C. Considering that 0.55% of cardiovascular mortality and 0.64% of respiratory mortality were attributable to global fire $PM_{2.5}$ exposure during 2000–2016 (Chen et al., 2021), the enhancement in the risk of mortality associated with fire air pollution could be greatly constrained by limiting global warming to 1.5 °C compared to that in a stronger warming world.

Our projections are also influenced by some uncertainties and limitations. First, potential uncertainties in climate change may affect future estimates of fire activities. Using one single model may cause uncertainties in future meteorology and LAI projections owing to internal variabilities or systematic biases (Brunner et al., 2020). The predicted warming is in general consistent with the MME from CMIP6 models (Fig. S6) while the predicted changes in precipitation show larger variability than the CMIP6 MME (Fig. S7). More climate-vegetable models ought to be selected and inter-compared to reduce uncertainties. Second, the impacts of changes caused by land use and land cover are not considered. YIBs uses fixed land cover and does not account for the PFT competitions. As a result, biomass burning from land use activities is not included in future projections. However, the assumptions of future anthropogenic land use are highly uncertain under different scenarios (Stehfest et al., 2019). Because 1.5 °C and 2 °C warmings might be achieved in the near future, land cover changes would likely have smaller effects on fire activity on this timescale (Neumann et al., 2021). Third, some important processes related to fire activities are ignored in the fire parameterization used in this study. For example, the wind is an essential variable affecting the spread of fires but is not considered in the parameterization. LAI is selected to characterize fuel availability but fuel types and structures are not considered. Other factors such as beetle outbreak (Kurz et al., 2008) and burning severity (Yue et al., 2015) may affect the availability of fuel load and the combustion completeness. In the future, we will incorporate more physical processes and possible feedbacks into the fire scheme to better predict fire regimes under global warming. Finally, ozone formation is dependent on the ratio between VOCs and NO_x ($NO + NO_2$). The increases in NO_x emissions from fires are not necessarily enhancing surface O_3, especially over some urban areas with the VOC-limited regime. Such nonlinear impacts on the population exposure to fire O_3 should be further explored using finer-resolution atmospheric chemical models in future studies.

5. Conclusions

We use the climate-chemistry-vegetation coupled model ModelE2-YIBs to project future changes in fire emissions under 1.5 °C and 2 °C warmings, taking into account the joint impacts of climate, vegetation, and human activities. Global fire emissions of different atmospheric components will increase by 10.0%–15.4% (15.1%–22.5%) in the 1.5 °C (2 °C) warmer world. The most significant increases are located in South America, southern Africa, and boreal Eurasia, while reductions are projected in the Sahel. Higher VPD promotes fuel dryness and a warmer climate elongates fire seasons, both of which provide favorable climatic conditions for more fires. However, higher population density in central Africa induces stronger fire suppressions and the consequent reductions of fire activities in the Sahel. The fire-induced air pollutants mainly follow the changes in emissions, leading to increases in population-weighted exposure to $PM_{2.5}$ by 5.1% and surface O_3 by 10.2% in the 1.5 °C warming period compared to present day. The additional half-degree warming will largely increase the $PM_{2.5}$ and O_3 exposure by 13% and 16% respectively, suggesting the large benefit of reducing fire-related air pollution by limiting global warming to 1.5 °C.

Author contributions statement

XY conceived the study. XY and CT designed the research and performed the model runs. CT completed data analysis and the first draft. XY reviewed and edited the manuscript. JZ, HL, YY, and LC advised on concepts and methods. XZ, YL, HZ and YC helped with data collection. All authors contributed to the discussion of the results and to the finalization of the paper.

Declaration of competing interest

The authors declare that they have no known competing financial interests or personal relationships that could have appeared to influence the work reported in this paper.

Data availability

Data will be made available on request.

Acknowledgements

This work was supported by the National Key Research and Development Program of China (grant nos 2022YFE0106500, 2019YFA0606802).

Appendix A. Supplementary data

Supplementary data to this article can be found online at https://doi.org/10.1016/j.envpol.2023.121311.

References

Abatzoglou, J.T., Williams, A.P., Barbero, R., 2019. Global emergence of anthropogenic climate change in fire weather indices. Geophys. Res. Lett. 46, 326–336.
Andela, N., Morton, D.C., Giglio, L., Chen, Y., van der Werf, G.R., Kasibhatla, P.S., DeFries, R.S., Collatz, G.J., Hantson, S., Kloster, S., Bachelet, D., Forrest, M.,

Lasslop, G., Li, F., Mangeon, S., Melton, J.R., Yue, C., Randerson, J.T., 2017. A human-driven decline in global burned area. Science 356, 1356.
Aragão, L.E.O.C., Malhi, Y., Barbier, N., Lima, A., Shimabukuro, Y., Anderson, L., Saatchi, S., 2008. Interactions between rainfall, deforestation and fires during recent years in the Brazilian Amazonia. Phil. Trans. Biol. Sci. 363, 1779–1785.
Archibald, S., Roy, D.P., Van Wilgen, B.W., Scholes, R.J., 2009. What limits fire? An examination of drivers of burnt area in Southern Africa. Global Change Biol. 15, 613–630.
Arino, O., Rosaz, J.-M., Goloub, P., 1999. The ATSR world fire atlas. A synergy with 'polder' aerosol products. Earth Obs. Q. 64, 1–6.
Batllori, E., Parisien, M.-A., Krawchuk, M.A., Moritz, M.A., 2013. Climate change-induced shifts in fire for Mediterranean ecosystems. Global Ecol. Biogeogr. 22, 1118–1129.
Bowman, D.M.J.S., Balch, J.K., Artaxo, P., Bond, W.J., Carlson, J.M., Cochrane, M.A., D'Antonio, C.M., DeFries, R.S., Doyle, J.C., Harrison, S.P., Johnston, F.H., Keeley, J. E., Krawchuk, M.A., Kull, C.A., Marston, J.B., Moritz, M.A., Prentice, I.C., Roos, C.I., Scott, A.C., Swetnam, T.W., van der Werf, G.R., Pyne, S.J., 2009. Fire in the earth system. Science 324, 481.
Bradstock, R.A., 2010. A biogeographic model of fire regimes in Australia: current and future implications. Global Ecol. Biogeogr. 19, 145–158.
Brunner, L., Pendergrass, A.G., Lehner, F., Merrifield, A.L., Lorenz, R., Knutti, R., 2020. Reduced global warming from CMIP6 projections when weighting models by performance and independence. Earth Syst. Dynam. 11, 995–1012.
Carvalho, A., Flannigan, M.D., Logan, K.A., Gowman, L.M., Miranda, A.I., Borrego, C., 2009. The impact of spatial resolution on area burned and fire occurrence projections in Portugal under climate change. Climatic Change 98, 177.
Chadburn, S.E., Burke, E.J., Cox, P.M., Friedlingstein, P., Hugelius, G., Westermann, S., 2017. An observation-based constraint on permafrost loss as a function of global warming. Nat. Clim. Change 7, 340–344.
Chen, G., Guo, Y., Yue, X., Tong, S., Gasparrini, A., Bell, M.L., Armstrong, B., Schwartz, J., Jaakkola, J.J.K., Zanobetti, A., Lavigne, E., Nascimento Saldiva, P.H., Kan, H., Royé, D., Milojevic, A., Overcenco, A., Urban, A., Schneider, A., Entezari, A., Vicedo-Cabrera, A.M., Zeka, A., Tobias, A., Nunes, B., Alahmad, B., Forsberg, B., Pan, S.-C., Íñiguez, C., Ameling, C., De la Cruz Valencia, C., Åström, C., Houthuijs, D., Van Dung, D., Samoli, E., Mayvaneh, F., Sera, F., Carrasco-Escobar, G., Lei, Y., Orru, H., Kim, H., Holobaca, I.-H., Kyselý, J., Teixeira, J.P., Madureira, J., Katsouyanni, K., Hurtado-Díaz, M., Maasikmets, M., Ragettli, M.S., Hashizume, M., Stafoggia, M., Pascal, M., Scortichini, M., de Sousa, Zanotti, Stagliorio Coêlho, M., Valdés Ortega, N., Ryti, N.R.I., Scovronick, N., Matus, P., Goodman, P., Garland, R. M., Abrutzky, R., Garcia, S.O., Rao, S., Fratianni, S., Dang, T.N., Colistro, V., Huber, V., Lee, W., Seposo, X., Honda, Y., Guo, Y.L., Ye, T., Yu, W., Abramson, M.J., Samet, J.M., Li, S., 2021. Mortality risk attributable to wildfire-related $PM_{2.5}$ pollution: a global time series study in 749 locations. Lancet Planet. Health 5, e579–e587.
Chen, J., Dai, A., Zhang, Y., Rasmussen, K.L., 2020. Changes in convective available potential energy and convective inhibition under global warming. J. Clim. 33, 2025–2050.
Chen, Y., Morton, D.C., Andela, N., van der Werf, G.R., Giglio, L., Randerson, J.T., 2017. A pan-tropical cascade of fire driven by El Niño/Southern Oscillation. Nat. Clim. Change 7, 906–911.
Clark, S.K., Ward, D.S., Mahowald, N.M., 2017. Parameterization-based uncertainty in future lightning flash density. Geophys. Res. Lett. 44, 2893–2901.
Dennison, P.E., Brewer, S.C., Arnold, J.D., Moritz, M.A., 2014. Large wildfire trends in the western United States, 1984–2011. Geophys. Res. Lett. 41, 2928–2933.
Eyring, V., Bony, S., Meehl, G.A., Senior, C.A., Stevens, B., Stouffer, R.J., Taylor, K.E., 2016. Overview of the coupled model intercomparison project phase 6 (CMIP6) experimental design and organization. Geosci. Model Dev. (GMD) 9, 1937–1958.
Flannigan, M., Cantin, A.S., de Groot, W.J., Wotton, M., Newbery, A., Gowman, L.M., 2013. Global wildland fire season severity in the 21st century. For. Ecol. Manag. 294, 54–61.
Flannigan, M., Stocks, B.J., Wotton, B.M., 2000. Climate change and forest fires. Sci. Total Environ. 262, 221–229.
Fonseca, M.G., Alves, L.M., Aguiar, A.P.D., Arai, E., Anderson, L.O., Rosan, T.M., Shimabukuro, Y.E., de Aragão, L.E.O.e.C., 2019. Effects of climate and land-use change scenarios on fire probability during the 21st century in the Brazilian Amazon. Global Change Biol. 25, 2931–2946.
Friedlingstein, P., O'Sullivan, M., Jones, M.W., Andrew, R.M., Hauck, J., Olsen, A., Peters, G.P., Peters, W., Pongratz, J., Sitch, S., Le Quéré, C., Canadell, J.G., Ciais, P., Jackson, R.B., Alin, S., Aragão, L.E.O.C., Arneth, A., Arora, V., Bates, N.R., Becker, M., Benoit-Cattin, A., Bittig, H.C., Bopp, L., Bultan, S., Chandra, N., Chevallier, F., Chini, L.P., Evans, W., Florentie, L., Forster, P.M., Gasser, T., Gehlen, M., Gilfillan, D., Gkritzalis, T., Gregor, L., Gruber, N., Harris, I., Hartung, K., Haverd, V., Houghton, R.A., Ilyina, T., Jain, A.K., Joetzjer, E., Kadono, K., Kato, E., Kitidis, V., Korsbakken, J.I., Landschützer, P., Lefèvre, N., Lenton, A., Lienert, S., Liu, Z., Lombardozzi, D., Marland, G., Metzl, N., Munro, D.R., Nabel, J.E.M.S., Nakaoka, S.I., Niwa, Y., O'Brien, K., Ono, T., Palmer, P.I., Pierrot, D., Poulter, B., Resplandy, L., Robertson, E., Rödenbeck, C., Schwinger, J., Séférian, R., Skjelvan, I., Smith, A.J.P., Sutton, A.J., Tanhua, T., Tans, P.P., Tian, H., Tilbrook, B., van der Werf, G., Vuichard, N., Walker, A.P., Wanninkhof, R., Watson, A.J., Willis, D., Wiltshire, A.J., Yuan, W., Yue, X., Zaehle, S., 2020. Global carbon budget 2020. Earth Syst. Sci. Data 12, 3269–3340.
Gao, J., 2017. Downscaling Global Spatial Population Projections from 1/8-degree to 1-km Grid Cells.
Gao, J., 2020. Global 1-km Downscaled Population Base Year and Projection Grids Based on the Shared Socioeconomic Pathways, Revision 01. NASA Socioeconomic Data and Applications Center (SEDAC) (Palisades, NY).
Gates, W.L., Boyle, J.S., Covey, C., Dease, C.G., Doutriaux, C.M., Drach, R.S., Fiorino, M., Gleckler, P.J., Hnilo, J.J., Marlais, S.M., Phillips, T.J., Potter, G.L., Santer, B.D., Sperber, K.R., Taylor, K.E., Williams, D.N., 1999. An overview of the results of the atmospheric model intercomparison project (AMIP I). Bull. Am. Meteorol. Soc. 80, 29–56.
Giglio, L., Kendall, J.D., Mack, R., 2003. A multi-year active fire dataset for the tropics derived from the TRMM VIRS. Int. J. Rem. Sens. 24, 4505–4525.
Giglio, L., Randerson, J.T., van der Werf, G.R., 2013. Analysis of daily, monthly, and annual burned area using the fourth-generation global fire emissions database (GFED4). J. Geophys. Res.: Biogeosciences 118, 317–328.
Girardin, M.P., Mudelsee, M., 2008. Past and future changes in CANADIAN boreal wildfire activity. Ecol. Appl. 18, 391–406.
Gong, C., Lei, Y., Ma, Y., Yue, X., Liao, H., 2020. Ozone–vegetation feedback through dry deposition and isoprene emissions in a global chemistry–carbon–climate model. Atmos. Chem. Phys. 20, 3841–3857.
Groot, W.J.d., Bothwell, P.M., Carlsson, D.H., Logan, K.A., 2003. Simulating the effects of future fire regimes on western Canadian boreal forests. J. Veg. Sci. 14, 355–364.
Guo, M., Li, J., Xu, J., Wang, X., He, H., Wu, L., 2017. CO2 emissions from the 2010 Russian wildfires using GOSAT data. Environ. Pollut. 226, 60–68.
Hantson, S., Arneth, A., Harrison, S.P., Kelley, D.I., Prentice, I.C., Rabin, S.S., Archibald, S., Mouillot, F., Arnold, S.R., Artaxo, P., Bachelet, D., Ciais, P., Forrest, M., Friedlingstein, P., Hickler, T., Kaplan, J.O., Kloster, S., Knorr, W., Lasslop, G., Li, F., Mangeon, S., Melton, J.R., Meyn, A., Sitch, S., Spessa, A., van der Werf, G.R., Voulgarakis, A., Yue, C., 2016. The status and challenge of global fire modelling. Biogeosciences 13, 3359–3375.
Hsu, N.C., Si-Chee, T., King, M.D., Herman, J.R., 2004. Aerosol properties over bright-reflecting source regions. IEEE Trans. Geosci. Rem. Sens. 42, 557–569.
Jahn, A., 2018. Reduced probability of ice-free summers for 1.5 °C compared to 2 °C warming. Nat. Clim. Change 8, 409–413.
Jiang, Y., Yang, X.-Q., Liu, X., Qian, Y., Zhang, K., Wang, M., Li, F., Wang, Y., Lu, Z., 2020. Impacts of wildfire aerosols on global energy budget and climate: the role of climate feedbacks. J. Clim. 33, 3351–3366.
Johnston, F.H., Henderson, S.B., Chen, Y., Randerson, J.T., Marlier, M., DeFries, R.S., Kinney, P., Bowman, D.M.J.S., Brauer, M., 2012. Estimated Global Mortality Attributable to Smoke from Landscape Fires 120, 695–701.
Jolly, W.M., Cochrane, M.A., Freeborn, P.H., Holden, Z.A., Brown, T.J., Williamson, G.J., Bowman, D.M.J.S., 2015. Climate-induced variations in global wildfire danger from 1979 to 2013. Nat. Commun. 6, 7537.
Kaufman, Y.J., Wald, A.E., Remer, L.A., Bo-Cai, G., Rong-Rong, L., Flynn, L., 1997. The MODIS 2.1-/spl mu/m channel-correlation with visible reflectance for use in remote sensing of aerosol. IEEE Trans. Geosci. Rem. Sens. 35, 1286–1298.
King, A.D., Karoly, D.J., Henley, B.J., 2017. Australian climate extremes at 1.5 °C and 2 °C of global warming. Nat. Clim. Change 7, 412.
Knorr, W., Dentener, F., Hantson, S., Jiang, L., Klimont, Z., Arneth, A., 2016. Air quality impacts of European wildfire emissions in a changing climate. Atmos. Chem. Phys. 16, 5685–5703.
Knorr, W., Dentener, F., Lamarque, J.F., Jiang, L., Arneth, A., 2017. Wildfire air pollution hazard during the 21st century. Atmos. Chem. Phys. 17, 9223–9236.
Krawchuk, M.A., Moritz, M.A., Parisien, M.-A., Van Dorn, J., Hayhoe, K., 2009. Global pyrogeography: the current and future distribution of wildfire. PLoS One 4, e5102.
Kurz, W.A., Dymond, C.C., Stinson, G., Rampley, G.J., Neilson, E.T., Carroll, A.L., Ebata, T., Safranyik, L., 2008. Mountain pine beetle and forest carbon feedback to climate change. Nature 452, 987–990.
Lei, Y., Yue, X., Liao, H., Zhang, L., Yang, Y., Zhou, H., Tian, C., Gong, C., Ma, Y., Gao, L., Cao, Y., 2021. Indirect contributions of global fires to surface ozone through ozone–vegetation feedback. Atmos. Chem. Phys. 21, 11531–11543.
Levy, R.C., Mattoo, S., Munchak, L.A., Remer, L.A., Sayer, A.M., Patadia, F., Hsu, N.C., 2013. The Collection 6 MODIS aerosol products over land and ocean. Atmos. Meas. Tech. 6, 2989–3034.
Li, F., Lawrence, D.M., Bond-Lamberty, B., 2017. Impact of fire on global land surface air temperature and energy budget for the 20th century due to changes within ecosystems. Environ. Res. Lett. 12, 044014.
Li, Y., Mickley, L.J., Liu, P., Kaplan, J.O., 2020. Trends and spatial shifts in lightning fires and smoke concentrations in response to 21st century climate over the national forests and parks of the western United States. Atmos. Chem. Phys. 20, 8827–8838.
Liu, Y., Stanturf, J., Goodrick, S., 2010. Trends in global wildfire potential in a changing climate. For. Ecol. Manag. 259, 685–697.
Liu, Z., Wimberly, M.C., 2016. Direct and indirect effects of climate change on projected future fire regimes in the western United States. Sci. Total Environ. 542, 65–75.
Marlier, M.E., DeFries, R.S., Voulgarakis, A., Kinney, P.L., Randerson, J.T., Shindell, D.T., Chen, Y., Faluvegi, G., 2013. El Niño and health risks from landscape fire emissions in southeast Asia. Nat. Clim. Change 3, 131–136.
Myhre, G., Govaerts, Y., Haywood, J.M., Berntsen, T.K., Lattanzio, A., 2005. Radiative effect of surface albedo change from biomass burning. Geophys. Res. Lett. 32.
Neumann, J.E., Amend, M., Anenberg, S., Kinney, P.L., Sarofim, M., Martinich, J., Lukens, J., Xu, J.-W., Roman, H., 2021. Estimating PM2.5-related premature mortality and morbidity associated with future wildfire emissions in the western US. Environ. Res. Lett. 16, 035019.
Pechony, O., Shindell, D.T., 2009. Fire parameterization on a global scale. J. Geophys. Res. 114.
Price, C., 2009. Will a drier climate result in more lightning? Atmos. Res. 91, 479–484.
Randerson, J.T., Chen, Y., van der Werf, G.R., Rogers, B.M., Morton, D.C., 2012. Global burned area and biomass burning emissions from small fires. J. Geophys. Res.: Biogeosciences 117.
Schleussner, C.F., Lissner, T.K., Fischer, E.M., Wohland, J., Perrette, M., Golly, A., Rogelj, J., Childers, K., Schewe, J., Frieler, K., Mengel, M., Hare, W., Schaeffer, M.,

2016. Differential climate impacts for policy-relevant limits to global warming: the case of 1.5 °C and 2 °C. Earth Syst. Dynam. 7, 327–351.
Schmidt, G.A., Kelley, M., Nazarenko, L., Ruedy, R., Russell, G.L., Aleinov, I., Bauer, M., Bauer, S.E., Bhat, M.K., Bleck, R., Canuto, V., Chen, Y.-H., Cheng, Y., Clune, T.L., Del Genio, A., de Fainchtein, R., Faluvegi, G., Hansen, J.E., Healy, R.J., Kiang, N.Y., Koch, D., Lacis, A.A., LeGrande, A.N., Lerner, J., Lo, K.K., Matthews, E.E., Menon, S., Miller, R.L., Oinas, V., Oloso, A.O., Perlwitz, J.P., Puma, M.J., Putman, W.M., Rind, D., Romanou, A., Sato, M., Shindell, D.T., Sun, S., Syed, R.A., Tausnev, N., Tsigaridis, K., Unger, N., Voulgarakis, A., Yao, M.-S., Zhang, J., 2014. Configuration and assessment of the GISS ModelE2 contributions to the CMIP5 archive. J. Adv. Model. Earth Syst. 6, 141–184.
Silva, P.S., Bastos, A., Libonati, R., Rodrigues, J.A., DaCamara, C.C., 2019. Impacts of the 1.5 °C global warming target on future burned area in the Brazilian Cerrado. For. Ecol. Manag. 446, 193–203.
Smolyakov, B.S., Makarov, V.I., Shinkorenko, M.P., Popova, S.A., Bizin, M.A., 2014. Effects of Siberian wildfires on the chemical composition and acidity of atmospheric aerosols of remote urban, rural and background territories. Environ. Pollut. 188, 8–16.
Son, R., Kim, H., Wang, S.-Y., Jeong, J.-H., Woo, S.-H., Jeong, J.-Y., Lee, B.-D., Kim, S.H., LaPlante, M., Kwon, C.-G., Yoon, J.-H., 2021. Changes in fire weather climatology under 1.5 °C and 2.0 °C warming. Environ. Res. Lett. 16, 034058.
Stehfest, E., van Zeist, W.-J., Valin, H., Havlik, P., Popp, A., Kyle, P., Tabeau, A., Mason-D'Croz, D., Hasegawa, T., Bodirsky, B.L., Calvin, K., Doelman, J.C., Fujimori, S., Humpenöder, F., Lotze-Campen, H., van Meijl, H., Wiebe, K., 2019. Key determinants of global land-use projections. Nat. Commun. 10, 2166.
Tanré, D., Kaufman, Y.J., Herman, M., Mattoo, S., 1997. Remote sensing of aerosol properties over oceans using the MODIS/EOS spectral radiances. J. Geophys. Res. Atmos. 102, 16971–16988.
Tian, C., Yue, X., Zhou, H., Lei, Y., Ma, Y., Cao, Y., 2021. Projections of changes in ecosystem productivity under 1.5 °C and 2 °C global warming. Global Planet. Change, 103588.
Tian, C., Yue, X., Zhu, J., Liao, H., Yang, Y., Lei, Y., Zhou, X., Zhou, H., Ma, Y., Cao, Y., 2022. Fire–climate interactions through the aerosol radiative effect in a global chemistry–climate–vegetation model. Atmos. Chem. Phys. 22, 12353–12366.
Turco, M., Rosa-Cánovas, J.J., Bedia, J., Jerez, S., Montávez, J.P., Llasat, M.C., Provenzale, A., 2018. Exacerbated fires in Mediterranean Europe due to anthropogenic warming projected with non-stationary climate-fire models. Nat. Commun. 9, 3821.
van der Werf, G.R., Randerson, J.T., Giglio, L., van Leeuwen, T.T., Chen, Y., Rogers, B.M., Mu, M., van Marle, M.J.E., Morton, D.C., Collatz, G.J., Yokelson, R.J., Kasibhatla, P. S., 2017. Global fire emissions estimates during 1997–2016. Earth Syst. Sci. Data 9, 697–720.
Ward, D.S., Kloster, S., Mahowald, N.M., Rogers, B.M., Randerson, J.T., Hess, P.G., 2012. The changing radiative forcing of fires: global model estimates for past, present and future. Atmos. Chem. Phys. 12, 10857–10886.
Wu, C., Venevsky, S., Sitch, S., Mercado, L.M., Huntingford, C., Staver, A.C., 2021. Historical and future global burned area with changing climate and human demography. One Earth 4, 517–530.
Yang, C.-E., Fu, J.S., Liu, Y., Dong, X., Liu, Y., 2022. Projections of future wildfires impacts on air pollutants and air toxics in a changing climate over the western United States. Environ. Pollut. 304, 119213.
Yin, Y., Bloom, A.A., Worden, J., Saatchi, S., Yang, Y., Williams, M., Liu, J., Jiang, Z., Worden, H., Bowman, K., Frankenberg, C., Schimel, D., 2020. Fire decline in dry tropical ecosystems enhances decadal land carbon sink. Nat. Commun. 11, 1900.
Yue, X., Mickley, L.J., Logan, J.A., 2014. Projection of wildfire activity in southern California in the mid-twenty-first century. Clim. Dynam. 43, 1973–1991.
Yue, X., Mickley, L.J., Logan, J.A., Hudman, R.C., Martin, M.V., Yantosca, R.M., 2015. Impact of 2050 climate change on North American wildfire: consequences for ozone air quality. Atmos. Chem. Phys. 15, 10033–10055.
Yue, X., Strada, S., Unger, N., Wang, A., 2017. Future inhibition of ecosystem productivity by increasing wildfire pollution over boreal North America. Atmos. Chem. Phys. 17, 13699–13719.
Yue, X., Unger, N., 2015. The Yale Interactive terrestrial Biosphere model version 1.0: description, evaluation and implementation into NASA GISS ModelE2. Geosci. Model Dev. (GMD) 8, 2399–2417.
Yue, X., Unger, N., 2018. Fire air pollution reduces global terrestrial productivity. Nat. Commun. 9, 5413.
Zou, Y., Wang, Y., Qian, Y., Tian, H., Yang, J., Alvarado, E., 2020. Using CESM-RESFire to understand climate–fire–ecosystem interactions and the implications for decadal climate variability. Atmos. Chem. Phys. 20, 995–1020.